Monomer-Level Description of Stress and Birefringence Relaxation in Polymer Melts

J. Gao and J. H. Weiner*

Division of Engineering, Brown University, Providence, Rhode Island 02912

Received September 24, 1993; Revised Manuscript Received November 27, 1993®

ABSTRACT: Theories for stress and birefringence relaxation in polymer melts are usually based on coarse-grained chain models in which each bead represents many mers. We here develop a physical picture of these processes on the monomer level. It makes use of an intrinsic coordinate system for each mer in which the bonds attached to that mer are fixed. It is shown, through a molecular dynamics simulation, that associated with each mer there is an intrinsic monomer stress (stresslet) that remains constant when referred to this coordinate system throughout the relaxation process and that it is through the randomization of the orientations of these stresslets that, at later times, the macroscopic stress decays. Birefringence decay is treated in a parallel manner and leads to a simple expression for C_r, the stress-optical coefficient in the rubbery regime, in terms of the monomer polarizability tensor and the intrinsic monomer stress tensor. Good agreement with experiment is found for C_r for the present simulation of a polyethylene-like model.

I. Introduction

Molecular theories of stress relaxation in polymer melts are generally based on Rouse and Rouse-like chain models.[1] Each bead of these model chains represents many mers of a real chain and each of its bonds or segments represents many actual bonds. These segments are assumed to act as entropic springs in tension. In equilibrium, segment orientation is isotropic and the segment tensile force gives rise to an isotropic stress. When a deformation, such as shear or elongation, is imposed on the melt, the segment orientation becomes anisotropic and the segment tensile force gives rise to an anisotropic or deviatoric stress. This stress will decay to zero as the chain vectors return to their equilibrium distribution and the segment orientation returns to isotropy.

Nonbonded interactions play an important, but limited, role in these molecular theories. Interchain interactions are modeled, as in the Langevin equation, by a friction constant and a random force, so that they contribute to the character of the chain dynamics and the return to equilibrium. Furthermore, excluded volume interactions permit chain entanglements, and theories incorporate their effects on chain dynamics in different ways, e.g., by invoking the reptation concept and confining tubes. However, it is assumed that nonbonded interactions make only a hydrostatic or isotropic contribution to the stress; since only the deviatoric stress is of interest, they are not considered explicitly in this connection.

The production of optical birefringence in a melt by imposing a deformation and its subsequent decay are generally treated in a manner corresponding to that used for stress. From a knowledge of the monomer polarizability, the segment polarizability is computed, with cylindrical symmetry about the segment axis assumed. The polarizability of the melt then follows from a knowledge of segment orientation. In other treatments,[2] the segment polarizability is used to compute the polarizability of an entire chain as a function of the chain end-to-end vector. The polarizability of the melt is then computed from the chain vector distribution corresponding to a given deformation.

Coarse-grained theories of this type have been very successful in providing understanding of many aspects of polymer melt behavior, particularly the scaling of various phenomena with chain length. We are concerned here with a different goal, with gaining a physical picture of the nature of stress development and relaxation on the monomer level. That is, if we think of a polymer melt as a liquid of mers, each interacting with its neighbors through bonded and nonbonded interactions, how can we describe stress development and relaxation from the local viewpoint of an observer riding on a given mer? Is the picture roughly the same as that provided by the coarse-grained theory, with a bead of that theory representing a monomer and a segment representing a covalent bond?

We have been exploring this question in both equilibrium and nonequilibrium dense polymer systems through the computer simulation of various models. In this paper, we wish to demonstrate the utility in nonequilibrium processes of the concept of intrinsic monomer stresses previously introduced by us[3] for equilibrium systems.[4] We restrict attention to polyethylene-like model systems.

The plan of the paper is as follows: In section II we present the chain model and simulation procedure we employ. We then, in section III, review the intrinsic monomer stress concept and demonstrate, through simulation, its utility in stress-relaxation processes. In section IV we take up the phenomenon of birefringence development and decay, using the same framework for a treatment on the monomer level as previously employed for the study of stress. Finally, in section V, we contrast the monomer-level description of these processes developed here with the coarse-grained models and consider the implications of these differences.

II. Simulation Method

Chain Model. The chain model we employ in the simulation of stress relaxation in dense melts is motivated by the recent work of Takeuchi and Roe.[5] These authors performed extensive computer simulation studies of polymer melts, one consisting of polyethylene-like chains (PE model) and the other of freely-rotating chains (FRC model) in which the torsional potential of the PE model was turned off. We utilize the FRC model in the present work.

We next summarize the potentials and parameters of the FRC model. The monomers of this model chain are treated as united atoms. These are subjected to the bond

® Abstract published in *Advance ACS Abstracts,* February 1, 1994.

0024-9297/94/2227-1201$04.50/0

stretching potential

$$u_b(r) = {}^1/_2\kappa_b(r-a)^2 \quad (1)$$

where a is the zero-force bond length, and the bond-angle bending potential

$$u_\theta(\theta) = {}^1/_2\kappa_\theta(\cos\theta - \cos\theta_0)^2 \quad (2)$$

In addition, a truncated Lennard-Jones potential

$$u_{nb}(r) = 4\epsilon[(\sigma/r)^{12} - (\sigma/r)^6] \quad \text{for } r \le r_0$$
$$= u_{nb}(r_0) \quad \text{for } r \ge r_0 \quad (3)$$

is used for all interchain and intrachain nonbonded interactions, the latter acting between all mers separated by more than three bonds. The parameter values used by Takeuchi and Roe[5] are as follows: bond length $a = 0.152$ nm, $\kappa_b = 3.46 \times 10^4$ kJ nm^{-2} mol^{-1}, $\kappa_\theta = 5.00 \times 10^2$ kJ mol^{-1}, $\cos\theta_0 = -{}^1/_3$, $\sigma = 0.380$ nm, $r_0 = 1.5\sigma$, and $\epsilon = 0.5$ kJ mol^{-1}. By consideration of the variation with temperature of the volume of the system at constant pressure, Takeuchi and Roe determined its glass transition temperature as $T_g = 39$ K. The parameter values listed lead, for the CH_2 monomer, to the following conversion factors used in this paper: time unit $(m\sigma^2/\epsilon)^{1/2} = 2.01$ ps and stress unit $\epsilon/\sigma^3 = 15.1$ MPa. The simulations employed a time step $\Delta t = 0.006$ ps.

Deformed Melt. We consider a dense melt of chains, consisting of ν chains confined to a volume v. This melt is subjected to a time-dependent deformation. We briefly outline the simulation procedure employed. Further details may be found in refs 6–8.

Periodic boundary conditions are employed in the molecular dynamics simulation in which the basic cell is a rectangular parallelepiped with dimensions L_1, L_2, and L_3 in the x_1, x_2, and x_3 coordinate directions, with $L_1 = L_2 = L_3 = L$ in the reference state. A given time-dependent deformation is imposed on the system by subjecting the basic cell to this deformation. Interactions between atoms in the basic cell with image atoms across the cell wall then serve to transmit the deformation to the atoms in the basic cell. In addition, a velocity increment corresponding to a velocity gradient equivalent to the constant-volume elongation at rate $\dot\epsilon_0$ is added to all the mer velocities at $t = 0$. (This combination of cell deformation and initial velocity gradient increment makes the simulation procedure for our deformation history equivalent to the SLLOD method of Evans and Morriss.[9])

The simulation reported here corresponds to a constant-volume elongation at rate $\dot\epsilon_0$ in the x_1 direction. That is

$$L_1(t) = \lambda_1(t)L, \quad L_2(t) = \lambda_2(t)L, \quad L_3(t) = \lambda_3(t)L \quad (4)$$

where

$$\lambda_1(t) = 1 + \dot\epsilon_0 t, \quad \lambda_2(t) = \lambda_3(t) = (\lambda_1(t))^{-1/2} \quad (5)$$

Constant-Temperature Algorithm. To maintain a constant temperature in the melt during deformation, we employ the velocity scaling algorithm due to Berendsen, Postma, van Gunsteren, DiNola, and Haak[10] and employed also by Brown and Clarke[11] in their simulations of the time-dependent mechanical behavior of dense polymer systems. We refer to the paper by Berendsen et al.[10] for the motivation of their procedure. The final algorithm for the determination of the atomic position $\mathbf{x}(t + \Delta t)$ in terms of the earlier positions $\mathbf{x}(t)$ and $\mathbf{x}(t - \Delta t)$ takes form

$$\mathbf{x}(t+\Delta t) = \mathbf{x}(t) + \xi\left(\mathbf{v}(t - {}^1/_2\Delta t) + \frac{\mathbf{f}}{m}\Delta t\right)\Delta t \quad (6)$$

where

$$\mathbf{v}(t - {}^1/_2\Delta t) = (\mathbf{x}(t) - \mathbf{x}(t-\Delta t))/\Delta t \quad (7)$$

the force $\mathbf{f}$ acting on the atom in question is determined for atomic positions at time t, and the velocity scaling factor

$$\xi = \left[1 + \frac{\Delta t}{\tau_T}\left(\frac{T_0}{T(t - {}^1/_2\Delta t)} - 1\right)\right]^{1/2} \quad (8)$$

where the temperature $T(t - {}^1/_2\Delta t)$ is based on the atomic velocities at $t - {}^1/_2\Delta t$ as computed from eq 7. Appropriate values of the parameter τ_T are discussed by Brown and Clarke.[12] Since our simulation used a high strain rate of $\dot\epsilon_0 = 0.01$ ps^{-1}, we found it necessary to use a value of $\tau_T = 50\Delta t$.

Ensemble Averages. The simulation is repeated for a large number (typically 90) of independent initial conditions. (In arriving at 90 initial configurations, we start with 30 independent configurations and permute the coordinate directions for each.) Time-dependent properties, such as the stress in the system corresponding to a particular deformation history, are obtained as an ensemble average over all of the 90 simulation runs. The simulation uses $\nu = 36$ chains with $N = 40$ bonds each. The basic cell volume $v = (12.855a)^3$, corresponding to a mass density $\rho = 0.938$ g/cm^3.

Virial Stress Formula. The form that the virial stress formula takes in the presence of the three-body bond-angle bending potential $u_\theta(\theta)$ is[8]

$$vt_{ij} = -\mu kT\delta_{ij} + \sum_{\alpha\in b}\langle r_\alpha^{-1}u'_b(r_\alpha)r_{\alpha i}r_{\alpha j}\rangle + \sum_{\alpha\in nb}\langle r_\alpha^{-1}u'_{nb}(r_\alpha)r_{\alpha i}r_{\alpha j}\rangle + \sum_m\langle C_{ij}(m)\rangle \quad (9)$$

where t_{ij} are the components of the stress tensor (force per unit present area) referred to the fixed rectangular Cartesian system x_i, $i = 1, 2, 3$, μ is the number of mers, δ_{ij} is the Kronecker delta, angular brackets denote an ensemble average, the prime denotes the derivative, $\mathbf{r}_\alpha$ is the vector displacement between the α pair with components $r_{\alpha i}$, $r_\alpha = |\mathbf{r}_\alpha|$, and the notations $\alpha \in$ b and $\alpha \in$ nb indicate that the sums range over all pairs of bonded or nonbonded interacting atom pairs, respectively. The quantity $C_{ij}(m)$ represents the bond angle contribution

$$C_{ij}(m) = -u'_\theta(\cos\theta_m)\left[\frac{r_{mi}r_{m+1j} + r_{mj}r_{m+1i}}{r_m r_{m+1}} + \left(\frac{r_{mi}r_{mj}}{r_m^2} + \frac{r_{m+1i}r_{m+1j}}{r_{m+1}^2}\right)\cos\theta_m\right] \quad (10)$$

where the sum ranges over all mers m of the system, excepting the end mers of each chain. The vector $\mathbf{r}_m$, with components r_{mi}, denotes the first bond (as measured from an arbitrary chain end) directly connected to mer m and it is pointing to the mer m. Similarly, the vector $\mathbf{r}_{m+1}$ is the second bond directly connected to mer m and pointing away from it (Figure 3).

We will generally be interested in the anisotropic portion of t_{ij}, that is, in the deviatoric stress tensor ${}^Dt_{ij}$ defined as

$${}^Dt_{ij} = t_{ij} - {}^1/_3\delta_{ij}t_{kk} \quad (11)$$

where here and throughout we are adopting the summation convention with respect to repeated Latin indices. Note that ${}^Dt_{11} = {}^2/_3(t_{11} - {}^1/_2(t_{22} + t_{33}))$ and we will find it convenient to use this quantity, and the analogous quantity

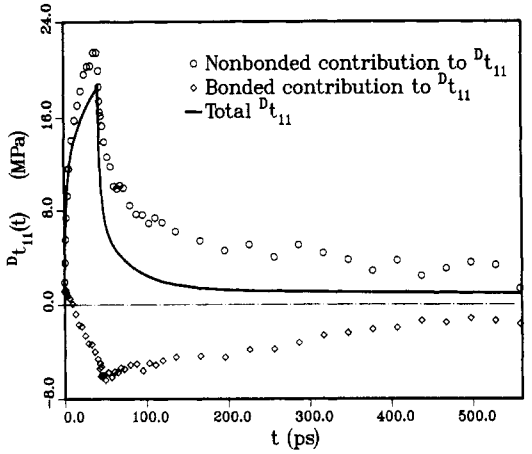

Figure 1. Deviatoric stress $^{D}t_{11}$ in the melt as determined by simulation in response to constant-volume elongation in the x_1 direction at the rate $\dot{\epsilon}_0 = 0.01$ ps^{-1} for $t \leq 42$ ps, followed by unloading with $\dot{\epsilon}_0 = 0.0$. Data points are shown for the nonbonded and bonded contributions to $^{D}t_{11}$ but omitted for their sum for clarity. (See Figure 7 for a repeat of the fitted curve for $^{D}t_{11}(t)$ together with the data points.) The numerical procedure for fitting the curve for the total $^{D}t_{11}$ and for the remaining fitted curves is described in refs 6 and 7.

for other tensors, to describe the anisotropy in a system undergoing the deformation of eqs 4 and 5.

Simulation Results. We have performed a simulation in which the deformation of eq 5 is applied for $0 < t < t_1$ (loading period) followed by an unloading period, $\dot{\epsilon}_0 = 0$ for $t \geq t_1$ where $t_1 = 42$ ps. (In the simulation, a velocity increment corresponding to a velocity gradient equivalent to the constant-volume elongation at rate $-\dot{\epsilon}_0$ is added to all the mer velocities at $t = t_1$.) The results for $^{D}t_{11}$ are shown in Figure 1. Of particular interest to us in the present connection is the dominant contribution made by the nonbonded interactions, as compared to the contributions of the covalent potentials. The fitting of a smooth curve through the simulation data here and in remaining figures involves the nonlinear determination of parameters in a Prony series; details are given in refs 6 and 7.

III. Intrinsic Stress Concept

We rewrite the virial stress formula, eq 9, in the form

$$\frac{vt_{ij}(t)}{kT} = \sum_m \langle \sigma_{ij}(m,t) \rangle \tag{12}$$

where the sum is over all mers of the system and

$$\sigma_{ij}(m,t) = \frac{1}{kT}\left[\frac{1}{2}\sum_{\alpha(m)} r_\alpha^{-1} u'_{b}(r_\alpha) r_{\alpha i} r_{\alpha j} + \frac{1}{2}\sum_{\alpha(m)} r_\alpha^{-1} u'_{nb}(r_\alpha) r_{\alpha i} r_{\alpha j} + C_{ij}(m,t)\right] - \delta_{ij} \tag{13}$$

for all mers, excepting the end mers of each chain where the angle term $C_{ij}(m,t)$ is omitted; the sums in eq 13 are over all pairs α interacting with mer m. We speak of $\sigma_{ij}(m,t)$ as the mer stress with its components referred to the fixed laboratory frame x_i; it is the contribution that mer m makes at time t to the nondimensionalized macroscopic stress vt_{ij}/kT.

As we have seen in our previous simulation studies, the nonbonded interactions make an anisotropic contribution to the stress because the interactions with a given mer are sterically screened by adjacent mers that are bonded to the given mer. The screening process is shown schematically in Figure 2. It is therefore logical to refer the mer stress to a local coordinate system in which the covalent bonds to mer m are fixed. We follow the same convention as in our previous work.[3] It is summarized in what follows.

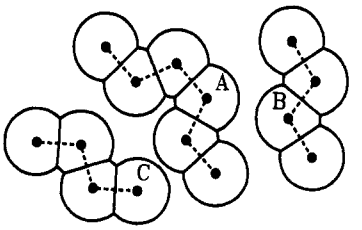

Figure 2. Schematic representation of the steric screen of nonbonded interactions that is responsible for their anisotropic stress contribution. Mer A interacts more readily with mer B than with mer C because of steric interference by mers bonded to A.

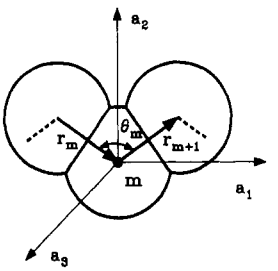

Figure 3. Base vectors $\mathbf{a}_1$, $\mathbf{a}_2$, and $\mathbf{a}_3$ for intrinsic coordinate system for mer m. Bond vectors $\mathbf{r}_m$ and $\mathbf{r}_{m+1}$ lie in the $\mathbf{a}_1$,$\mathbf{a}_2$ plane.

Intrinsic Monomer-Level Stresses. For every chain-interior mer m, we introduce a moving local Cartesian coordinate system whose unit base vectors $\mathbf{a}_i$, $i = 1,2,3$, are defined in terms of the bond vectors $\mathbf{r}_m$ and $\mathbf{r}_{m+1}$ attached to m as follows (Figure 3):

$$\mathbf{a}_1 = \left(\frac{\mathbf{r}_{m+1}}{r_{m+1}} + \frac{\mathbf{r}_m}{r_m}\right)(2(1 - \cos\theta_m))^{-1/2}$$

$$\mathbf{a}_2 = \left(\frac{\mathbf{r}_{m+1}}{r_{m+1}} - \frac{\mathbf{r}_m}{r_m}\right)(2(1 + \cos\theta_m))^{-1/2} \tag{14}$$

$$\mathbf{a}_3 = \mathbf{a}_1 \times \mathbf{a}_2$$

with θ_m the bond angle at mer m. For a chain-end mer m, $\mathbf{a}_1$ is parallel to the end bond connected to the end mer m and directed from m toward the mer bonded to it, and $\mathbf{a}_3$ is chosen to be the same as that of the mer bonded to mer m; $\mathbf{a}_2$ is then equal to $\mathbf{a}_3 \times \mathbf{a}_1$.

Let $\mathbf{e}_i$, $i = 1,2,3$, be the unit base vectors of the fixed laboratory reference frame. Then any vector $\mathbf{r}$ can be written in terms of components with respect to either frame as $\mathbf{r} = r_i\mathbf{e}_i = \bar{r}_j\mathbf{a}_j$, where we are adopting throughout the convention that superposed bars denote components with respect to the local frame $\mathbf{a}_i$. The vector components with respect to the two frames are related in the usual way as

$$r_i = \bar{r}_j \mathbf{a}_j \cdot \mathbf{e}_j = \bar{r}_j a_{ji} \tag{15}$$

where $a_{ji} = \mathbf{a}_j \cdot \mathbf{e}_i$, with inverse relation,

$$\bar{r}_j = r_i a_{ij}^{-1} \tag{16}$$

where $a_{ij}^{-1} = \mathbf{e}_i \cdot \mathbf{a}_j = a_{ji}$.

Similarly, the monomer-level stress tensor can be expressed in terms of components with respect to either

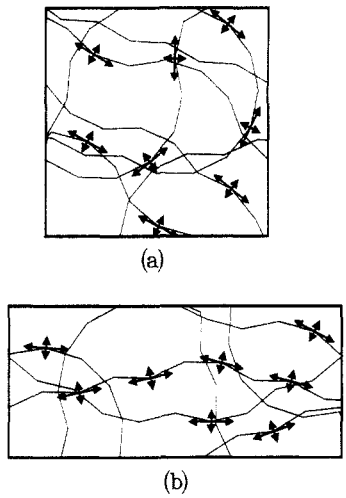

Figure 4. Schematic representation of intrinsic monomer stress (stresslet) associated with some representative mers. They are all identical except for orientation. (a) In the undeformed reference state, the stresslet orientation is randomly distributed and their macroscopic sum is an isotropic stress. (b) Under deformation, they acquire a preferred orientation and their macroscopic sum is anisotropic.

frame as $\sigma(m) = \sigma_{ij}\mathbf{e}_i\mathbf{e}_j = \bar{\sigma}_{rs}\mathbf{a}_r\mathbf{a}_s$ with the tensor components related as

$$\sigma_{ij} = \bar{\sigma}_{rs}a_{ri}a_{sj} \tag{17}$$

$$\bar{\sigma}_{rs} = \sigma_{ij}a_{ir}^{-1}a_{js}^{-1} = \sigma_{ij}a_{ri}a_{sj} \tag{18}$$

where, for mer m, $a_{ri}(m,t) = \mathbf{a}_r(m,t)\cdot\mathbf{e}_i$ is the transformation matrix for the moving coordinate system attached to mer m at time t. With this convention on the significance of $a_{ri}(m,t)$, by the use of eq 17 we can rewrite eq 12 in terms of intrinsic stresses as

$$\frac{vt_{ij}(t)}{kT} = \sum_m \langle \bar{\sigma}_{rs}(m,t)a_{ri}(m,t)a_{sj}(m,t)\rangle \tag{19}$$

as an ensemble average of a sum over all mers in the basic cell.

Our previous work employing the concept of intrinsic monomer stress dealt with an equilibrium model for a polymer network. There we found that the intrinsic monomer stress was relatively independent of the degree of deformation and had the same value as in the corresponding equilibrium un-cross-linked melt. This result led to the physical picture of a network in which each mer was the bearer of a stresslet.[13] The stresslets are, except for orientation, all identical (ignoring chain end effects for the moment). In the equilibrium isotropic state, the stresslets are randomly oriented and therefore the macroscopic stress is zero. Stretching the network causes a partial ordering of the stresslet orientation and therefore leads to a nonzero macroscopic stress. In this ordering process, the magnitudes of the stresslet principal values remain unchanged. This process is illustrated schematically in Figure 4.

We now test the applicability of this concept to the nonequilibrium deformation process simulated in the previous section. During the simulation we compute the components of the monomer orientation matrix $a_{ri}(m,t)$ and of the ensemble-averaged intrinsic monomer stress $\langle\bar{\sigma}_{rs}(m,t)\rangle$. The values of the latter averaged over all interior mers are shown in Figure 5. It is seen there that although the macroscopic stress components t_{ij} (which are, of course, referred to the fixed laboratory frame) are undergoing large variations, the intrinsic monomer stresses

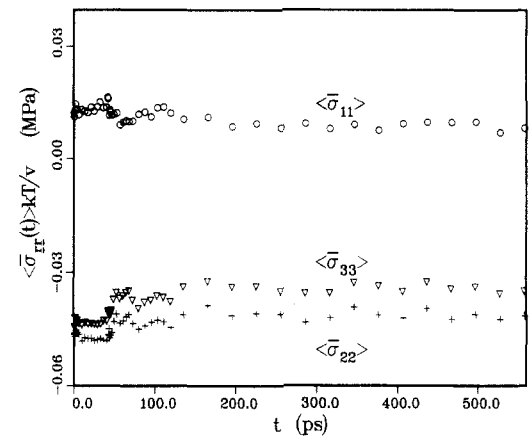

Figure 5. Time variation of intrinsic monomer stress components $\langle\bar{\sigma}_{rr}(t)$ (no sum) for the same loading history that gives rise to the macroscopic stress variation ${}^{D}t_{11}(t)$ shown in Figure 1. Components are averaged over the central chain mers (mers 5–35) to avoid end effects (see Figure 6). Equilibrium melt results for these quantities agree with unloading period results within statistical scatter.

$\langle\bar{\sigma}_{rs}(m,t)\rangle$ are essentially time-independent. (There are small differences in these quantities during the loading period ($0 < t < t_1 = 42$ ps when $\dot{\epsilon}_0 > 0$) and unloading period ($t > t_1$ when $\dot{\epsilon}_0 = 0$), but these differences are small compared to the variations in t_{ij}.) Furthermore, their values remain the same as in an equilibrium melt. Therefore, the concept and physical picture for these intrinsic stresses retain their significance in nonequilibrium processes.

Although the intrinsic monomer stresses $\langle\bar{\sigma}_{rs}\rangle$ are time-independent, there is a chain end region dependence. A typical example is shown in Figure 6. Therefore, we refer to these quantities by the notation $\langle\bar{\sigma}_{rs}(m)\rangle$; for polyethylene-like systems of sufficiently long chains, this mer dependence may be neglected.

We return to eq 19 and rewrite it in the form (which follows directly from the ensemble average concept)

$$\frac{vt_{ij}}{kT} = \sum_m \langle\bar{\sigma}_{rs}(m)\rangle\langle a_{ri}(m,t)a_{sj}(m,t)\rangle + \sum_m \langle\delta\bar{\sigma}_{rs}(m,t)\delta A_{risj}(m,t)\rangle \tag{20}$$

where

$$\delta\bar{\sigma}_{rs}(m,t) = \bar{\sigma}_{rs}(m,t) - \langle\bar{\sigma}_{rs}(m)\rangle \tag{21}$$

$$\delta A_{risj}(m,t) = a_{ri}(m,t)a_{sj}(m,t) - \langle a_{ri}(m,t)a_{sj}(m,t)\rangle \tag{22}$$

Consider the significance of the first sum in eq 20. The quantities $\langle\bar{\sigma}_{rs}(m)\rangle$ represent the time-independent components (with respect to the intrinsic coordinate system) of the stresslet associated with mer m. The first sum represents, therefore, the macroscopic stress due to the orientation of these mers through the orientation matrix $\langle a_{ri}(m,t)a_{sj}(m,t)\rangle$. We refer to this macrocopic stress as the orientation stress, $t_{ij}^{O}(t)$; it arises from the partial orientation of the monomer stresslets. That is

$$t_{ij}^{O} = \frac{kT}{v}\sum_m \langle\bar{\sigma}_{rs}(m)\rangle\langle a_{ri}(m,t)a_{sj}(m,t)\rangle \tag{23}$$

In Figure 7 we plot ${}^{D}t_{11}^{O}$. It is seen that at later times ${}^{D}t_{11}^{O}$ agrees well with ${}^{D}t_{11}$, but it substantially underestimates the deviatoric stress during the loading period. In other words, the second sum in eq 20 represents a means of stress production that is in addition to the orienting

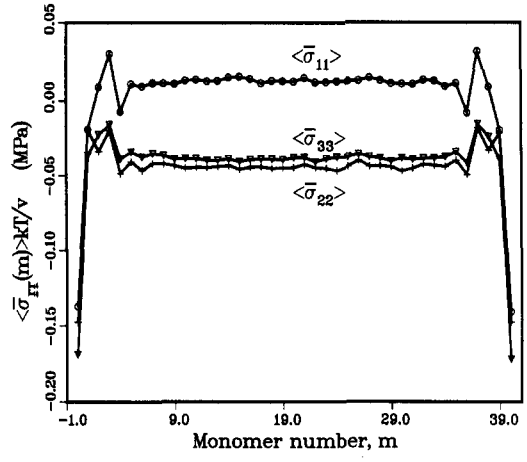

Figure 6. Variation along chain of intrinsic stress components $\langle\bar{\sigma}_{rr}(m)\rangle$ (no sum). Results shown represent time average period 48–128 ps.

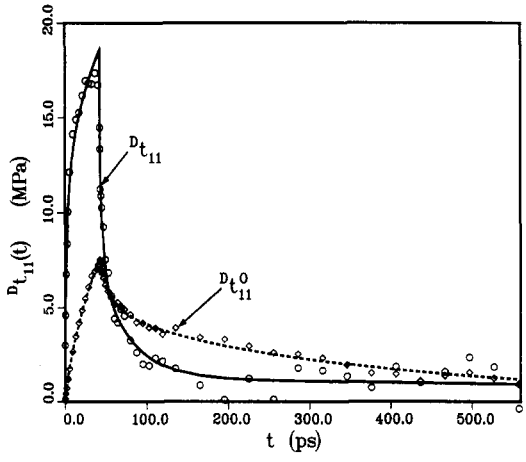

Figure 7. Comparison of $^{D}t^{O}_{11}$, orientation stress (eq 23), with total deviatoric stress $^{D}t_{11}$.

stresslet mechanism. This second mechanism is dominant at early times after the imposition of the deformation but then rapidly decays. We refer to this mode of stress production as the affine mechanism and denote the stress due to it as t^{A}_{ij}. The motivation for this terminology is discussed next.

Affine Mechanism. We start with the time-dependent deformation of constant-volume elongation described by eq 5. To each initial configuration of mers in the ensemble, we apply the corresponding time-dependent affine deformation. Use of the resulting mer position in the virial stress formula, eq 9, then leads to a linearly increasing stress $^{D}t^{a}_{11}$. It is seen in Figure 8 that at extremely early times, the affine deformation causes stretching of covalent bonds and a very rapid rise in stress $^{D}t_{11}$ to which the linearly increasing stress $^{D}t^{a}_{11}$ is initially tangent. The highly stressed covalent bonds rotate to relieve this stress and the covalent contribution to $^{D}t_{11}$ then rapidly decreases.

Also shown in Figure 8 is $(^{D}t_{11})_{nb}$, the nonbonded contribution to $^{D}t_{11}$, together with $(^{D}t^{a}_{11})_{nb}$, the nonbonded contribution to $^{D}t^{a}_{11}$. It is seen that the linearly increasing $(^{D}t^{a}_{11})_{nb}$ is initially tangent to $(^{D}t_{11})_{nb}$. We conclude that the initial rapid rise in stress occurring after the start of the constant strain rate elongation is due to the motion of the mers of the system according to this time-dependent affine deformation; thermal motion of the mers plays no role in this very early period.

However, the actual stress rise follows the linear rise for only a very short period and then increases more slowly;

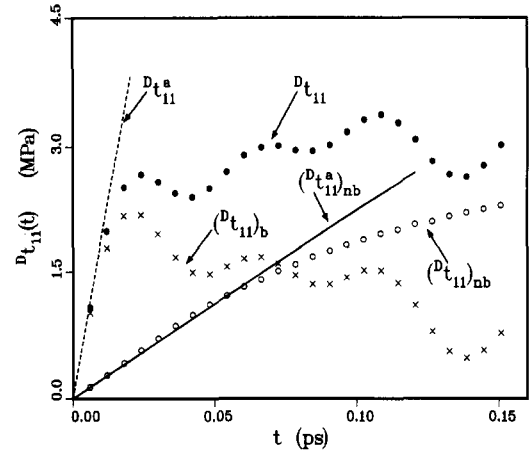

Figure 8. Early-time behavior of deviatoric stress $^{D}t_{11}$ together with $(^{D}t_{11})_{b}$ and $(^{D}t_{11})_{nb}$, the bonded and nonbonded contributions to this stress. Also shown is $^{D}t^{a}_{11}$, the value of this stress if all mers followed the macroscopic affine deformation, and $(^{D}t^{a}_{11})_{nb}$, the nonbonded contribution to this affine stress.

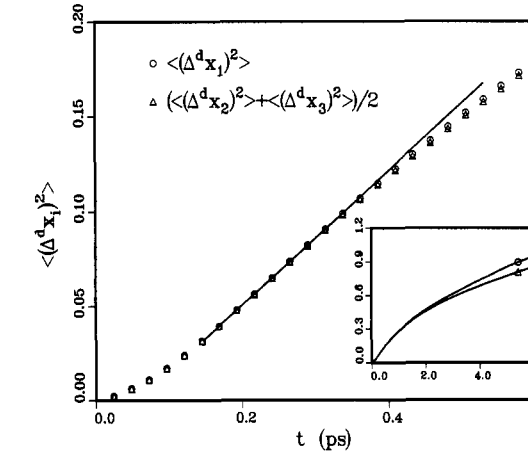

Figure 9. Early-time monomer self-diffusion from sites they would have occupied under an affine displacement corresponding to the macroscopic deformation as measured by $\langle(\Delta^{d}x_i)^2\rangle$, eq 25. The straight line is added to guide the eye. Insert for somewhat longer times shows that diffusion in the direction of extension, $i = 1$, is greater than in the transferve directions, $i = 2,3$.

this is seen most clearly in Figure 8 by comparing $(^{D}t_{11})_{nb}$ and $(^{D}t^{a}_{11})_{nb}$. We postulate that this occurs because under influence of thermal motion the system mers diffuse away from the affine positions they would have occupied in the absence of thermal motion. More specifically, we assume that a typical mer displacement

$$\Delta\mathbf{x}(t) = \mathbf{x}(t) - \mathbf{x}(0) \tag{24}$$

can be written as the sum

$$\Delta\mathbf{x}(t) = \Delta^{a}\mathbf{x}(t) + \Delta^{d}\mathbf{x}(t) \tag{25}$$

where $\Delta^{a}\mathbf{x}(t)$ is computed by means of the affine deformation, while $\Delta^{d}\mathbf{x}(t)$ is random, corresponding to self-diffusion. As a test of this hypothesis, the program computes $\langle(\Delta^{d}x_i)^2\rangle$ (t), $i = 1,2,3$, where $\Delta^{d}x_i$ are the components of $\Delta^{d}\mathbf{x}$ with respect to the x_1, x_2, and x_3 axes. These are shown in Figure 9 for the same simulation treated in the earlier figures. It is seen that, after a brief initial period $0 < t < 0.07$ ps, $\langle(\Delta^{d}x_i)^2\rangle$ (t) becomes linear in t as expected for diffusion of free monomers; however, by $t \approx 0.4$ ps, the bond constraints cause the diffusion to fall below the linear rate. (The time $t \approx 0.07$ ps when linear diffusion begins corresponds also (Figure 8) to the time when $(^{D}t_{11})_{nb}$ starts to fall below its linear variation.) It is also of interest to note that the rate of diffusion in the x_1

direction, the direction of the elongation, is slightly larger than in the transverse directions. This anisotropy is seen more clearly in records (see the insert of Figure 9) of $\langle(\Delta^d x_i)^2\rangle$ taken over longer periods of time.

We conclude, therefore, on the basis of these simulation results that the mode of stress mechanism which we have called the affine mechanism and designated by t_{ij}^A corresponds to a stress rise due to affine mer displacements accompanied by mer diffusion away from the affine sites. (Note that the symbol t_{ij}^a referred to the linear rise in stress due to the affine mer displacement unrelieved by subsequent diffusion.) We have observed this same mechanism operative in simulations of viscoelasticity of simple liquids[6,14] where, indeed, it is the only available mechanism for deviatoric stress production and relaxation. Although the nature of the affine mechanism is the same in polymer melts and simple liquids, stress relaxation in the latter is much more rapid because diffusion away from the affine sites is not hindered by a bond structure.

IV. Birefringence Relaxation

The concepts of mer intrinsic coordinate systems and their orientation matrices $a_{ri}(m,t)$ lend themselves directly to a discussion on the monomer level of melt polarizability and birefringence. Let $\bar{\alpha}_{rs}(m)$ be the components of the polarizability tensor of mer m referred to the intrinsic coordinate system for that mer. For a polymer such as polyethylene with side groups that have no additional degrees of freedom relative to the backbone chain, $\bar{\alpha}_{rs}$ can be taken as time-independent and, for our polyethylene-like model system, independent of m as well. We confine attention to this case here, although the method could be generalized to the case of time-dependent $\bar{\alpha}_{rs}$. Then $\beta_{ij}(t)$, the polarizability tensor of the melt referred to the laboratory frame during stress relaxation, is

$$\beta_{ij}(t) = \sum_m \bar{\alpha}_{rs}\langle a_{ri}(m,t)a_{sj}(m,t)\rangle \tag{26}$$

Since deviatoric tensors satisfy the same transformation laws as do the full tensors, it follows from eq 26 that

$$^D\beta_{ij}(t) = \sum_m {}^D\bar{\alpha}_{rs}\langle a_{ri}(m,t)a_{sj}(m,t)\rangle \tag{27}$$

We next restrict attention to mers of sufficient symmetry so that $^D\bar{\alpha}_{rs}$ is diagonal. Then

$$^D\beta_{11}(t) = \mu(^D\bar{\alpha}_{11}\langle\langle a_{11}^2\rangle\rangle(t) + {}^D\bar{\alpha}_{22}\langle\langle a_{21}^2\rangle\rangle(t) + {}^D\bar{\alpha}_{33}\langle\langle a_{31}^2\rangle\rangle(t)) \tag{28}$$

where μ is the number of mers in the system (μ = 1476 in this simulation) and $\langle\langle a_{11}^2\rangle\rangle(t)$ is the average of $\langle a_{11}^2(m,t)\rangle$ over all of the system mers, etc. For the following calculations representative of polyethylene, we use the values $\bar{\alpha}_{11}$ = 24.2, $\bar{\alpha}_{22}$ = 19.4, and $\bar{\alpha}_{33}$ = 14.6 for CH_2 monomers, all in units of 10^{-31} M^3. These have been obtained from the C–C and C–H bond polarizabilities[15] by tensor transformation.[16]

For an isotropic system, the Lorentz–Lorenz expression connecting the index of refraction n and the total polarizability β is

$$\frac{n^2-1}{n^2+2} = \frac{4\pi}{3}\frac{\beta}{v} \tag{29}$$

where v is the volume of the system. For a system with small anisotropy, we make the usual assumption that eq 29 may be applied to the principal components n_{11}, β_{11}, etc. so that we may write

$$n_{11} = \left(\frac{(8\pi/3v)\beta_{11}+1}{1-(4\pi/3v)\beta_{11}}\right)^{1/2} \tag{30}$$

with corresponding equations for the other principal components. With the assumption of small anisotropy, we can then approximate the birefringence $\Delta n = n_{11} - n_{22}$, or, equivalently, $^Dn_{11} = {}^2/_3(n_{11} - {}^1/_2(n_{22} + n_{33}))$, as

$$^Dn_{11} = \frac{2\pi}{9v}\frac{(n^2+2)^2}{n}\,{}^D\beta_{11} \tag{31}$$

where $n = {}^1/_3 n_{kk}$ is the mean refractive index.

Stress-Optical Coefficient. We can now compute the stress-optical coefficient $C(t)$ for the simulated system by use of the relation

$$C(t) = \frac{^Dn_{11}}{^Dt_{11}} = \frac{^Dn_{11}}{^Dt_{11}^A + {}^Dt_{11}^O} \tag{32}$$

The result is shown in Figure 10. It is seen that $C(t)$ begins with a relatively low value in the early glassy regime and rises by a factor of ca. 10 in the terminal regime. This is in qualitative agreement with what is observed experimentally.[17] In terms of the present physical picture, it is clear that this behavior is due to the initial large value of the affine stress $^Dt_{11}^A$ and to its rapid decay. It is also of interest to consider the orientational stress-optical coefficient $C_o(t)$ defined as

$$C_o(t) \triangleq \frac{^Dn_{11}}{^Dt_{11}^O} \tag{33}$$

This is shown in Figure 10 and is seen to be substantially constant throughout the loading and unloading process. This is not surprising, since the polarizability and the orientational stress both arise from monomer orientation.

We also note from Figure 10 that $C_o(t) \approx C(t)$ for later times due to the decay to zero of the affine stress $^Dt_{11}^A$. This suggests a further approximation to $C(t)$ for later times.

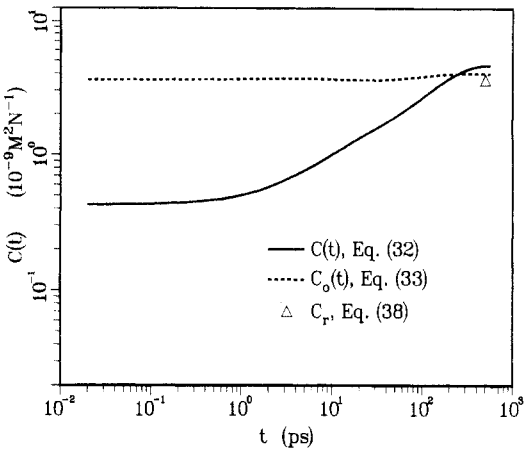

Figure 10. Stress-optical coefficient, $C(t)$, as determined from simulation. The fitted Prony series to stress and birefringence data are used, with the assumptions of linear viscoelasticity, to obtain the model behavior under constant strain rate loading with no unloading period. In the fitted Prony series[6,7] to the stress history $^Dt_{11}(t)$ for use in eq 32, the first mode corresponding to very early time bonding stretching as in Figure 8 has been omitted. If this mode is included, the value of $C(t)$ at $t = 2 \times 10^{-2}$ ps decreases to $C = 0.019 \times 10^{-9}$ M^2 N^{-1}; later values of $C(t)$ at t = 500 ps remain substantially unchanged. Also shown is $C_o(t)$, eq 33, and C_r, eq 38.

By use of the relation $a_{11}^2 + a_{21}^2 + a_{31}^2 = 1$ it is possible to rewrite eq 28 in the form

$$^{D}\beta_{11}(t) = \mu\left[\frac{1}{2}{}^{D}\bar{\alpha}_{11}(3\langle\langle a_{11}^2\rangle\rangle(t) - 1) + \frac{1}{2}({}^{D}\bar{\alpha}_{22} - {}^{D}\bar{\alpha}_{33})(\langle\langle a_{21}^2\rangle\rangle(t) - \langle\langle a_{31}^2\rangle\rangle(t))\right] \quad (34)$$

For later times and the quoted values of $\bar{\alpha}_{rs}$, it is found from the simultations that the second term on the right-hand side of eq 34 is small compared to the first and that a good approximation to $^{D}\beta_{11}(t)$ is

$$^{D}\beta_{11}(t) \approx \mu({}^{D}\bar{\alpha}_{11}P_2(\theta_{11}(t))) \quad (35)$$

where

$$P_2(\theta_{11}) = {}^1/_2(3\langle\langle a_{11}^2\rangle\rangle - 1) = {}^1/_2(3\langle\langle\cos^2\theta_{11}\rangle\rangle - 1) \quad (36)$$

with θ_{11} the angle between $\mathbf{a}_1$ and $\mathbf{e}_1$. A similar approximation may be made in eq 23 for $^{D}t_{11}^{O}$, namely

$$^{D}t_{11}^{O} \approx \frac{kT}{v}\mu(\langle{}^{D}\bar{\sigma}_{11}\rangle P_2(\theta_{11}(t))) \quad (37)$$

where $\langle{}^{D}\bar{\sigma}_{11}\rangle$ is obtained from the later-time data of Figure 5. Therefore, for later times, an approximate value for the stress-optical coefficient C is

$$C_r = \frac{2\pi}{9kT}\frac{(n^2+2)^2}{n}\frac{{}^{D}\bar{\alpha}_{11}}{\langle{}^{D}\bar{\sigma}_{11}\rangle} \quad (38)$$

The value of C_r is shown in Figure 10 and it is seen, in fact, to provide a good approximation to $C(t)$ for later times. Equation 38 therefore gives a new and physically transparent definition of the terminal stress-optical coefficient in terms of the two intrinsic monomeric properties, $^{D}\bar{\alpha}_{11}$ and $\langle{}^{D}\bar{\sigma}_{11}\rangle$. If we use the quoted value of $^{D}\bar{\alpha}_{11}$ and the values of $(kT/v)\langle{}^{D}\bar{\sigma}_{11}\rangle = 0.031$ MPa and $n = 1.52$ as obtained from the simulation, then eq 38 leads, for $T = 172$ K, to $C_r = 3.6 \times 10^{-9}$ M^2 N^{-1}. This may be compared with the experimental value[18] $C_r = 2.35 \times 10^{-9}$ M^2 N^{-1} for high-density polyethylenes of narrow molecular mass distribution at $T = 150$ °C. In view of the idealizations involved in the FRC model, this agreement is very encouraging.

V. Conclusion and Discussion

We have considered in this paper the computer simulation of a dense polymer melt subjected to a short loading period of constant strain rate extension, followed by an unloading period in which the deformation is held fixed. In this simulation we employed a chain model in which individual monomers retain their identity rather than a coarse-grained model in which many mers are lumped together in a single bead.

Our concern here has been to develop a liquid-like, monomer-level physical picture of the process. That is, from the viewpoint of an observer riding on a representative mer, interacting with its neighbors with covalent bonded interactions as well as with nonbonded interactions, we have attempted to clarify the mechanisms through which an anisotropic stress builds up and decays in response to the imposed deformation.

In the usual view of stress in a dense polymer system, it is assumed that the nonbonded interactions make only a hydrostatic or isotropic contribution to the stress. In contrast, these simulations show (Figure 1) that the nonbonded interactions are primarily responsible for the anisotropic stress. This surprising result is in agreement with previous simulations made by us in both equilibrium[30] and nonequilibrium[6-8] systems and with simulations by Fixman,[31] who employed a different model and algorithm.

We have found, furthermore, that the macroscopic stress $t_{ij}(t)$ can be expressed as a sum of two stress histories

$$t_{ij}(t) = t_{ij}^{A}(t) + t_{ij}^{O}(t) \quad (39)$$

where each represents a different mechanism and dominates in a different period of the process.

The first, $t_{ij}^{A}(t)$, is termed the affine stress. When the deformation first starts, it arises from a displacement of all mers that corresponds to the macroscopic affine deformation. This results in a rapid buildup of stress that then decays rapidly as the mers diffuse away from the affine sites they would have occupied in the absence of the thermal motion. The affine stress mechanism has little to do with the covalent structure of the melt. It occurs as well in simulations of the viscoelasticity of simple liquids.[6,14] In the latter, the decay of $t_{ij}^{A}(t)$ is much more rapid since the atoms are unconstrained by covalent bonds.

The second mechanism gives rise to a stress history $t_{ij}^{O}(t)$ that is termed the orientation stress. To describe this mechanism it is first convenient to introduce an intrinsic coordinate system for each mer that bears a fixed relation to the covalent structure attached to that mer. We find that, even in equilibrium, each mer bears a stresslet, an intrinsic monomer stress, that has constant components when referred to that mer's intrinsic coordinate system (Figure 3). The origin of this intrinsic monomer stress is the fact that the interaction of a given mer, say mer A (Figure 2), is screened by the adjacent mers bonded to mer A. Because of the nature of their origin, the intrinsic monomer stresses retain the same values (except for orientation) whether the melt is in undeformed equilibrium or is undergoing a nonequilibrium deformation process. In equilibrium, the various stresslets are isotropically oriented with respect to a fixed laboratory frame and therefore the macroscopic stress, which is their sum, is isotropic. When a deformation is applied, the orientation of the stresslets becomes anisotropic and so does the macroscopic stress. This orientation stress $t_{ij}^{O}(t)$ then decays as the stresslet orientation returns to isotropy.

The affine stress variation occurs on a more rapid time scale than that of the orientation stress, and in the later terminal stages of stress relaxation, only the latter is significant. Since, as seen in Figure 1, the nonbonded contribution to the macroscopic stress is dominant in the later as well as in the earlier stages of the relaxation process, it is clear that the nonbonded interactions make the dominant contributions to the stresslets as well. The anisotropy of stresslet orientation in the deformed system, however, is produced by the chain structure, i.e., through the bonded interactions (Figure 4).

A central role in the description of $t_{ij}^{O}(t)$ is the matrix $a_{rs}(m,t)$ that describes the orientation of the intrinsic coordinate system for mer m at time t relative to the fixed laboratory frame. Use of this concept also permits a parallel treatment on the monomer level of the rise and relaxation of melt birefringence. It leads to a simple formulation for the stress-optical coefficient that describes its behavior as the system relaxes from the glassy regime through the terminal regime. It also leads to an approximate expression for the stress-optical coefficient in the terminal regime in terms of intrinsic monomer properties.

Some additional observations regarding this work and its relation to other theories are appropriate here:

(1) While coarse-grained theories that employ Rouse and Rouse-like chain models appear to be effective numerical procedures for computing the stress in the later stages of relaxation, they do not supply even a qualitatively correct physical picture on the monomer level. Missing from a coarse-grained description is the central role of nonbonded interactions in producing anisotropic stress and the fact that covalent bonds are in compression[23] at the usual melt densities. It would be of great interest and importance to develop a derivation of a coarse-grained theory from a monomer-level description, one which explains why it provides a quantitative prediction of later-stage stress relaxation. (Such theories cannot be expected to be applicable at early times when the affine stress mechanism, which has little to do with the covalent structure, is dominant.)

(2) In coarse-grained theories of birefringence, the polarizability of a segment, which comprises many bonds, plays a central role. The segment polarizability tensor is assumed to be cylindrically symmetric with respect to **r**, the segment vector. A similar assumption is made regarding the segment stress tensor, regarded as due to a tensile force **f** parallel to **r**. Simulations we have performed in dense melts rendered anisotropic by a large extension show[19] that the second assumption is violated in the presence of chain–chain interaction. Under these conditions there are two significant directions for a given chain—the chain vector **R** and the direction of elongation **x**—and the principal axes of the chain stress do not include **R** or, equivalently, the chain force is not parallel[20] to **R**. These results, for the entire chain, should apply as well to the chain segment stress tensor and, we believe, to the segment polarizability tensor. Other methods[21] of calculations of melt birefringence begin with the monomer polarizability tensor (and are not coarse-grained in this sense) but do compute the polarizability of an isolated chain as a cylindrical tensor with respect to the chain vector **R**.

(3) The simulation has been performed at a temperature T = 172 K, well above T_g = 39 K for this model as determined by Takeuchi and Roe.[5] It is necessary to do so in order that the system passes through the glassy regime rapidly and so that a substantial amount of stress relaxation occurs within a practical period of computer simulation. There is a fundamental difference in the way the system passes through the glassy regime below and above T_g. Below T_g, it is trapped in potential wells and overcomes barriers at long time intervals through the process of thermal activation. Above T_g, presumably, the thermal motion has sufficient energy to overcome these barriers frequently, with perhaps little trapping. Nevertheless, we believe there is qualitative similarity in the glassy behavior, in spite of the radically different time scales. Encouraging from this viewpoint is that simulations of the FRC model[8] show time–temperature behavior that is in accord with the WLF equation.

(4) We have also performed viscoelastic simulations[22] for the PE model of Takeuchi and Roe[5] which contain rotational energy barriers omitted from the FRC model. The simulated behavior of the PE model was quite similar to that of the FRC model with the principal difference that the relevant range of temperature was shifted upward since its T_g = 201 K. However, the presence of rotational energy barriers complicates the discussion of intrinsic monomer stresses because the screening of different long-lived conformers, such as *tt* or *tg*, affects these stresses. We have studied this question[23] in connection with intrinsic monomer force components but have not yet done so for intrinsic monomer stresses.

(5) The FRC model is a united-atom model in which a CH_2 mer is represented by a single Lennard-Jones atom. We believe that the C and H atoms could be treated explicitly[24] within the same framework, with no basic change in the essential ideas.

(6) The existence of two distinct mechanisms of stress relaxation in polymer melts is well recognized. They are sometimes referred to as the energetic and entropic regimes.[17] In this connection it should be pointed out that the affine mechanism that we have identified would be operative as well in a hard-sphere simple liquid, a purely entropic system. The present decomposition $t_{ij}(t) = t_{ij}^{A}(t) + t_{ij}^{0}(t)$ also provides a monomer-level interpretation to the expression of the relaxing stress in a melt as a sum of glassy and rubbery components.[25-28]

The coarse-grained models of polymer melts create a special category of materials in terms of the unique character of the mechanism of stress production through the action of long chains acting as entropic springs. The present monomer-level description fits better into the framework employed for other materials. As we have noted, the affine mechanism applies directly to the viscoelasticity of simple liquids. The concept of atomic-level stresses has been employed with profit[29] in the study of glasses and crystalline solids. The sole new feature in polymer melts is the intrinsic character of monomer stresses and the orientability of the intrinsic coordinate systems by deformation due to the chain structure.

The entropic character of equilibrium rubber elasticity is well established by macroscopic experiments, and this fact is sometimes taken as convincing evidence that the entropic spring mechanism of coarse-grained theories represents the unique physical picture for this class of materials. It is well to emphasize that the present monomer-level picture applies as well to a polymer model that employs hard spheres and geometric constraints to describe the bond structure and represents, therefore, a purely entropic system. In an equilibrium deformation, as in a network, the orientational mechanism is the only operative one, and we conjecture that we may think of t_{ij}^{0} as due to the decrease of entropy associated with the orientational ordering accompanying deformation. A quantitative comparison of this viewpoint with the usual chain conformation entropy viewpoint remains for future work.

Acknowledgment. This work was supported by the Gas Research Institute (Contract 5091-260-2237) with the computations performed on the Cray C-90 at the Pittsburgh Supercomputing Center.

References and Notes

(1) Doi, M.; Edwards, S. F. *The Theory of Polymer Dynamics*; Clarendon: Oxford, 1986.
(2) Treloar, L. R. G. *The Physics of Rubber Elasticity*, 3rd ed.; Clarendon: Oxford, 1975.
(3) Gao, J.; Weiner, J. H. *J. Chem. Phys.* **1989**, *90*, 6749.
(4) A preliminary account of this research was given in: Gao, J.; Weiner, J. H. *Polym. Mater. Sci. Eng.* **1993**, *69*, 18.
(5) Takeuchi, H.; Roe, R.-J. *J. Chem. Phys.* **1991**, *94*, 7446, 7458.
(6) Gao, J.; Weiner, J. H. *Macromolecules* **1992**, *25*, 1348.
(7) Gao, J.; Weiner, J. H. *Macromolecules* **1992**, *25*, 3462.
(8) Gao, J.; Weiner, J. H. *J. Chem. Phys.* **1992**, *97*, 8698.
(9) Evans, D. J.; Morriss, G. P. *Statistical Mechanics of Non-equilibrium Liquids*; Academic Press: London, 1991; p 137.
(10) Berendsen, H.; Postma, J.; van Gunsteren, W.; DiNola, A.; Haak, J. R. *J. Chem. Phys.* **1984**, *81*, 3684.
(11) Brown, D.; Clarke, J. H. R. *Macromolecules* **1991**, *24*, 2075.

(12) Brown, D.; Clarke, J. H. R. *Comput. Phys. Commun.* **1991**, *62*, 368.
(13) We are borrowing this terminology from Brady (Brady, J. F. *J. Chem. Phys.* **1993**, *98*, 3335), who uses it in connection with discussion of colloidal suspensions.
(14) Gao, J.; Weiner, J. H., unpublished.
(15) Denbigh, K. G. *Trans. Faraday Soc.* **1940**, *36*, 936; see ref 2, pp 202–203, for discussions.
(16) Jernigan, R. L.; Flory, P. J. *J. Chem. Phys.* **1967**, *47*, 1999.
(17) Wimberger-Friedl, R.; De Bruin, J. D. *Rheol. Acta* **1991**, *30*, 419.
(18) Janeschitz-Kriegl, H. *Polymer Melt Rheology and Flow Birefringence*; Springer-Verlag: Berlin, 1983; p 113.
(19) Gao, J.; Weiner, J. H. *Macromolecules* **1991**, *24*, 1519.
(20) Gao, J.; Weiner, J. H. *Macromolecules* **1991**, *24*, 5179.
(21) See, for example: Flory, P. J. *Statistical Mechanics of Chain Molecules*; Interscience: New York, 1969; Chapter IX.
(22) Weiner, J. H.; Gao, J. *Modelling Simul. Mater. Sci. Eng.*, in press.
(23) Gao, J.; Weiner, J. H. *J. Chem. Phys.* **1993**, *98*, 8256.
(24) Yoon, D. Y.; Smith, G. D.; Matsuda, T. *J. Chem. Phys.* **1993**, *98*, 10037.
(25) Priss, L. S.; Vishnyakov, I. I.; Pavlova, I. P. *Int. J. Polym. Mater.* **1980**, *8*, 85.
(26) Read, B. E. *Polym. Eng. Sci.* **1983**, *23*, 835.
(27) Shimo, T.; Nagasawa, M. *Macromolecules* **1992**, *25*, 5026.
(28) Hwang, E. J.; Inone, T.; Osaki, K. *Polymer* **1993**, *34*, 1661.
(29) Vitek, V.; Egami, T. *Phys. Status Solidi* **1987**, *144*, 145.
(30) Gao, J.; Weiner, J. H. *Macromolecules* **1989**, *22*, 979.
(31) Fixman, M. *J. Chem. Phys.* **1991**, *95*, 1410.